Design, Synthesis and Molecular Modeling of Benzofuran-8-Hyroxyquinoline Hybrids as Multi-Target Inhibitors and Potential Anti-Alzheimer's Disease

Awwad Radwan *, Fars Alanazi, Anas M. Abdel Rahman

Posted Date: 13 February 2024

doi: 10.20944/preprints202402.0731.v1

Keywords: Benzofuran; Alzheimer's disease; AChEs; BChE; BACE1; docking study, Molecular dynamics simulations

Article

Design, Synthesis and Molecular Modeling of Benzofuran-8-Hyroxyquinoline Hybrids as Multi-Target Inhibitors and Potential Anti-Alzheimer's Disease

Awwad A. Radwan [1,*], Fars K. Alanazi [1] and Anas M. Abdel Rahman [2]

[1] Kayyli Chair for Pharmaceutical Industries, Department of Pharmaceutics, College of Pharmacy, King Saud University, P.O. Box 2457, Riyadh 11451, Saudi Arabia; aradwan@ksu.edu.sa; afars@ksu.edu.sa

[2] Metabolomics Section, the Department of Clinical Genomics, Center for Genome Medicine, King Faisal Specialist Hospital and Research Center, Riyadh, 11211, Saudi Arabia.; aabdelrahman46@kfshrc.edu.sa

* Correspondence: aradwan@ksu.edu.sa (AR)

Abstract: Cholinesterase (ChE) and secretase (BACE) inhibitors, and fibril- and β-amyloid-suppressing medicines are used to treat Alzheimer's disease (AD) symptomatically. The prevalence and complex nature of AD have increased the urgent need for multi-targeted directed ligands (MTDLs). This is because MTDLs can prevent potential drug-drug interactions during poly-therapy and have a better therapeutic profile than single targeted agents. Using piperazine linker or spacer and two primary scaffolds, benzofuran and 8-hydroxyquinoline, a unique class of multi-targeted medicines was recently reported by our group. These compounds showed remarkable effectiveness in inhibiting Aβ1-42 aggregation and acting as iron chelators.The results prompted us to synthesize an additional series of compounds as multimodal anti-AD agents and investigate its inhibitor activities to ChE (AChE/BChE) and BACE1 enzymes. The resulting inhibitory effects suggested that the compounds under study might be used to improve cognitive function. The docking analysis' findings revealed that the compounds bind to AChE and BChE by forming H-bond interactions with amino acid residues at binding sites and μ-stacking interactions with aromatic residues, whereas the binding to BACE1 only revealed H-bond interactions with amino acid residues at binding sites.

Keywords: benzofuran; Alzheimer's disease; AChEs; BChE; BACE1; docking study; molecular dynamics simulations

1. Introduction

A serious neurodegenerative brain condition, Alzheimer's disease (AD) is characterised by a decline in cognitive performance and ultimately, memory loss. The condition deteriorates with age. Ever since AD was formally diagnosed in 1910, it has been a persistent problem and a difficult sickness for medical experts worldwide to comprehend [1]. Over 55 million people worldwide suffer with dementia, and over 60% of them reside in low- or middle-income countries. According to data from https://www.who.int/news-room/fact-sheets/detail/dementia (accessed October 9, 2022), the proportion of older people in the population is rising in almost every nation. By 2030, it is expected that this number will rise to 78 million, and by 2050, it will reach 139 million. We still don't fully comprehend the pathophysiological pathways behind AD. Nonetheless, despite its complexity, four hypotheses, among others, can be used to identify a number of neurodegenerative pathways. 1. The aspartyl protease β-site APP cleaving enzyme-1 (BACE1) and γ-secretase progressively degrade amyloid precursor protein (APP) to produce insoluble amyloid beta (Aβ) plaques (Figure 1). 2. Tau protein hyperphosphorylation leads to intracellular accumulations of neurofibrillary tangles (NFTs) in neuronal and glial cells. 3. The pathology of AD is related to the biometals' malfunction that results in detrimental excess level of heavy metals such as copper and iron. 4. Oxidative stress causes brain

 doi:10.20944/preprints202402.0731.v1

neuronal cells to die and synapses to disappear [2]. High level in the inflammatory mediators and low level in the neurotransmitter acetylcholine (ACh) have a distinct role in AD pathology [3-5].

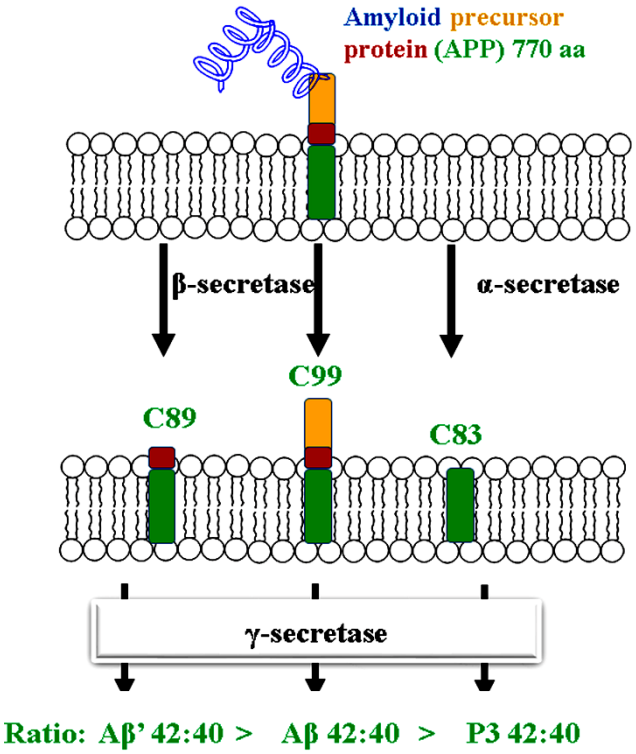

Figure 1. The biological development of β-amyloid protein AB1-42.

When acetylcholinesterase (AChE) is suppressed in the early stages of AD, ACh levels increase and cognitive function improves. As AD progresses and AChE levels are thought to be declining, AChE inhibitors (AChEIs) appears to be ineffective [6]. On the other hand, butyrylcholinesterase (BuChE) levels either remain constant or even increase [7] and BuChEIs are effective in the late stages of AD since BChEIs can hydrolyze ChE to compensate for the drop in AChE activity [8]. The intracellular buildup of hyperphosphorylated neurofibrillary tangles of tau protein, oxidative and inflammatory stresses are additional hypotheses that support the multifactorial character of AD illness [9,10]. The five subsites that make up the active sites of ChE enzymes are the catalytic active site (CAS), peripheral anionic site (PAS), acyl binding pocket, oxyanion hole, and anionic subsite [11]. One of the distinctions between the structure of both AChE and BuChE is the size of the acyl pocket. More specifically, the acyl pocket of BuChE has smaller residues like Leu286 and Val288 that enable a larger site, whereas the acyl pocket of AChE contains larger and more aromatic Phe295 and Phe297 residues that enable a smaller site. The aforementioned structural differences have an impact on selective inhibitor design [12]. The inhibition of Aβ peptide accumulation in the brain can be considered as a treatment strategy in delaying the start of AD [3]. Reduced plaque aggregation has been demonstrated to be a benefit of heavy metals (Cupper, Iron) chelators [13]. A common course of treatment for AD involves acetylcholinesterase inhibitors such donepezil (E2020, Aricept®), galantamine, and rivastigmine, which improve cholinergic neurotransmission [14]. Butyl choline esterase has been found to be a co-regulator of acetylcholine activity, which has recently attracted the attention of chemists and biologists who are concerned in the role of these enzymes in AD [15]. Given the complexity of AD, one gene change might not be sufficient to deliver the necessary treatment. Multi-targeted directed ligands (MTDLs) are now more important than ever to prevent interaction between multi-therapeutics drugs and to have a better therapeutic treatment than single-targeted therapy. This is due to the prevalence of Alzheimer disease (AD) in addition to the growing understanding of its multifactorial nature. In light of these results, the exciting notion of developing multi-target molecules may lead to a more effective therapeutic strategy [16]. Based on this new

Preprints.org (www.preprints.org) | NOT PEER-REVIEWED | Posted: 13 February 2024 doi:10.20944/preprints202402.0731.v1

paradigm, several researchers created a number of hybrid compounds, including SKF-64346 and derivatives of acridine (Figure 2). The alkylamine moiety of these hybrid medicines inhibits cholinesterase (AChE and BuChE), while the benzofuran or acridine motif inhibits Aβ-aggregation [17, 18]. Many compounds (Figure 2) were developed to exhibit antiaggregant and anticholinesterase activities [19]. HLA-20 (8-hydroxyquinoline derivatives) and M30's capacities to chelate iron, scavenge free radicals, and prevent iron-catalyzed lipid membrane peroxidation have all been proven [20, 21].

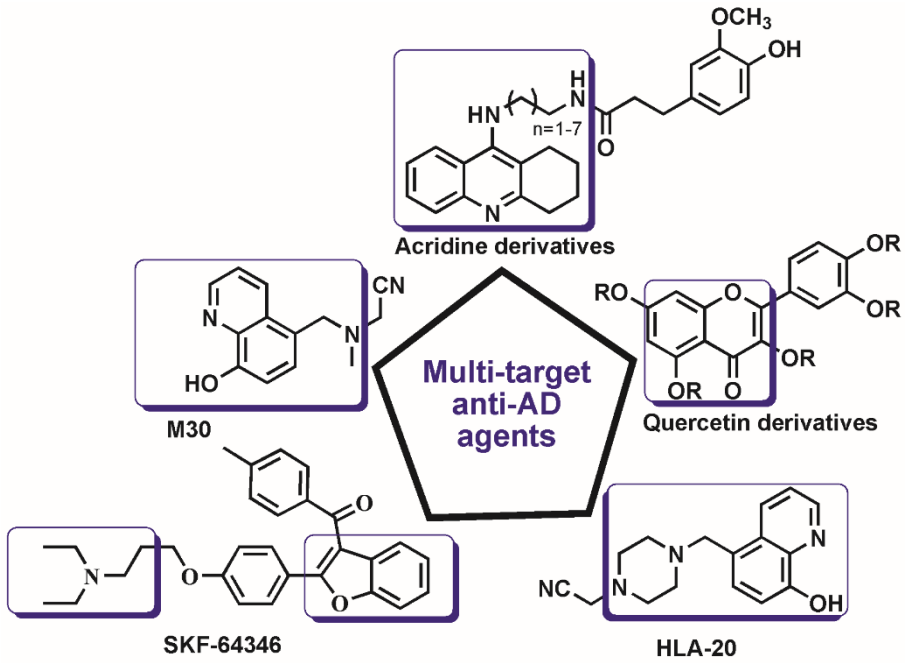

Figure 2. Representative compounds as multi-target anti-AD agents.

The lead compound SKF-64346, an AChE/BChE and γ-secretase inhibitor has motivated us to develop a number of hybrid molecules through linking the benzofuran and 8-hydroxyquinoline moieties by piperazine spacer that also facilitates BBB crossing. To assess the effect of the substitutes on the electrical configuration of the whole structure and their impact on the compounds' biological activity, a range of substitutions were introduced to position 2 of the benzofuran scaffold (Figure 3). Promising results obtained in our published work where the hybrid compounds explored significant inhibition of $A\beta_{1-42}$ self-aggregation and chelated bio-metals such as Fe^{3+} [24]. These findings prompted us continue our work for the synthesis of new derivatives and perform biological evaluation against more AD-target enzymes ChE 'including AChE/BChE' and BAC1.

 doi:10.20944/preprints202402.0731.v1

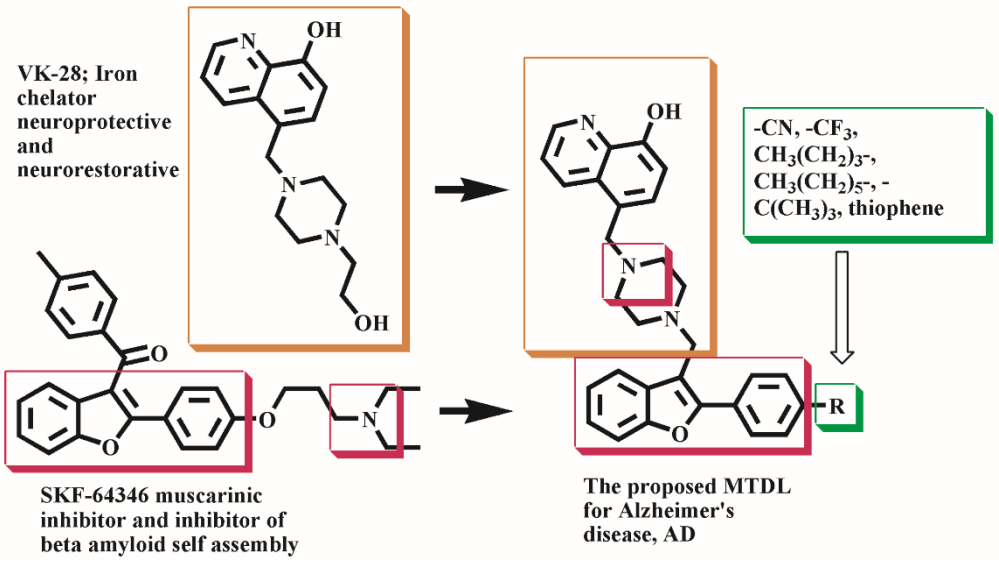

Figure 3. Schematic representation of the designed compounds.

2. Results and Discussions

2.1. Chemistry

The synthetic route for the intermediates and final compounds is depicted in scheme 1. The starting materials 5-chloromethyl-8-hydroxyquinoline hydrochloride **3** and 5-((piperazin-1-yl)methyl)quinolin-8-ol **5** [22, 23] were prepared according to reported procedures. Wittig reaction was utilized to prepare 2-Aryl[b]benzofurans intermediate compounds **8-14** through the reaction of 2-hydroxybenzyltriphenyl phosphonium bromide with substituted-benzoic acid chloride in aprotic solvent, toluene, and trimethylamine. Mannich reaction was utilized for aminoalkylation of compounds **8-14** with 5-((piperazin-1-yl)methyl)quinolin-8-ol revealing 5-((4-((2-(4-substitutedphenyl)benzofuran-3-yl)methyl)piperazin-1-yl)methyl)quinolin-8-ol final compounds **22-28**. Structure elucidations of compounds (**8-14**, **22-28**) was done using IR, ^{1}H NMR, ^{13}C NMR, mass spectral data and CHN analysis. Two distinctive bands were visible in the IR spectra of compounds **8-14** at 3095-2975 cm^{-1} due to aromatic CH stretching and at 868-725 cm^{-1} due to aromatic CH out-of-plane bending. Conversion of **8-14** into **22-28** leads to the development of new bands at 3378-3315 cm^{-1} related to phenolic OH stretching of the 8-hydroxyquinoline fragment. 1H NMR spectra of **8-14** revealed signals at δ 6.66–8.68 ppm characteristic of 2-phenylbenzofuran. Transformation of compounds **8-14** into compounds **22-28** resulted in emergence of new NMR signals due to aliphatic protons of both piperazine ring appeared as two signals at δ 2.55-291 and 2.68-2.98 ppm and two N-methylene protons at δ 3.51-3.81 and at 3.69-4.29 ppm. In additions, compounds **22-28** showed signals at chemical shift range δ 6.89-8.87 ppm. Moreover, the butyl-, pentyl- and hexyl substituents showed characteristic four-signals pattern at δ 0.85-0.93, 1.22-1.42, 1.56-1.67, and 2.58-2.66 ppm for the intermediate compounds **10, 12, 13** and the final compounds **24, 26, 27**. Compounds **11, 25** showed characteristic t-butyl group as strong singlet signal at δ 1.32-1.39 ppm. 13C NMR spectra of compounds **8-14** revealed distinguishing signals at δ 100.69-102.25 ppm because of benzofuran-C3 that disappeared upon C3-aminoalkylation into compounds **22-28**.

Preprints.org (www.preprints.org) | NOT PEER-REVIEWED | Posted: 13 February 2024 doi:10.20944/preprints202402.0731.v1

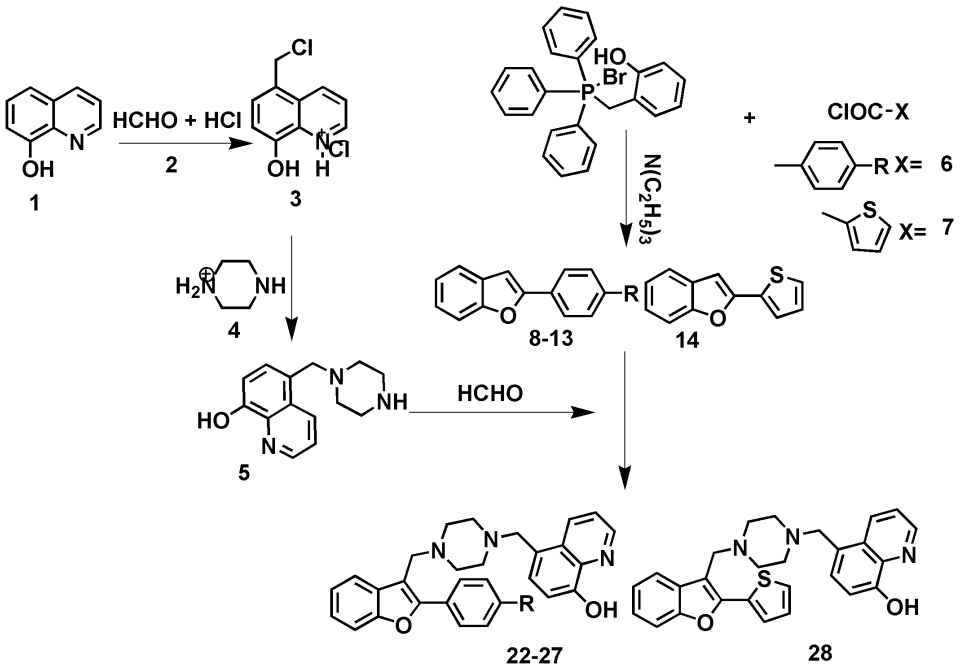

Scheme 1. The synthesis pathway. Reagents and conditions: (i) Et_3N, toluene, reflux 10 hrs; (ii) Formaline 37%, DMF, stir 3 hr at r.t. R = CN,**8,22**; CF_3, **9,23**; n-butyl, **10,24**; t-butyl, **11,25**; n-pentyl, **12,26**; n-hexyl, **13,27**.

2.2. Inhibition of AChE, BChE and BACE1 Activities

Table 1 displays moderate to strong in vitro inhibitory effects of compounds **15-28** against AChE and BChE. Compounds **15-28** explored an inhibition range of 33.4% - 81.3% against AChE while it showed an inhibition range of 54.58%-94.47% against BChE and an inhibition range of 20.9% - 97.9% against BACE1.

Table 1. Experimental and predicted AChE/BChE inhibition percent and docking scores of (10 μmol) compounds **15-28**.

No.	Binding Energy Kcalmol^{-1}		Inhibition constant (Ki nmol)		Experimental inhibition %	
	AChE	hBCHE	AChE	hBCHE	AChE	BChE
15	-14.83	-12.36	0.013	0.87	64.9	75.69
16	-15.32	-10.92	0.006	9.89	71.3	65.88
17	-14.37	-12.36	0.03	0. 87	58.2	91.53
18	-15.63	-12.97	0.004	0.31	79.9	94.47
19	-14.85	-12.64	0.013	0.54	64.1	86.65
20	-15.16	-11.82	0.008	2.17	68.5	74.35
21	-10.42	-11.61	23.1	3.07	50.8	72.7
22	-11.9	-11.03	1.89	8.22	81.3	84.06
23	-11.98	-10.91	1.66	10.03	69.6	54.58
24	-14.42	-11.88	0.027	1.96	74.4	80.77
25	-11.24	-13.79	5.78	0.08	74.4	78.73
26	-11.4	-12.23	4.38	1.09	47.8	74.95
27	-9.92	-11.78	53.13	2.34	60.8	79.18
28	-10.97	-12.75	9.07	0.45	33.8	67.57
Xray	-14.22	-11.38	0.038	4.55	----------	----------

 doi:10.20944/preprints202402.0731.v1

2.3. Docking Study of Compounds 15-28 against AChE and BChE Proteins Structures

Using Autodock4 [25], we were able to ascertain the molecular interactions and binding of the ligands **15–28** to AChE/BChE. The crystal structures of Torpedo California AChE (5nnu) [26] and human BChE(6i0b) [27] have been obtained through the protein database PDB. Before being docked to the macromolecule structure, the synthesized compounds **15–28** were sketched, optimized, and uploaded to pdbqt format. The experimental AChE/BChE-inhibition percent was in accordance with the docking scores (Table 1). For the complexes of compounds **15-28** with the protein structure, docking study has estimated the energy of binding in the range from -15.63 to -9.92 kcal mol^{-1} for AChE and -13.79 to -10.93 kcal mol^{-1} to BChE (Table 1) and revealed major contribution of hydrogen bonds and hydrophobic interactions (Table 2). Figure 4 shows the binders' docked poses inside the binding site and reveals the hydrogen-bonding residues to the ligands and the hydrophobic amino acids that are essential for ligand-target interactions. The interactions of compounds **15-28** with AChE showed hydrogen bonds to amino acid residues Tyr70, Tyr121, Ser122, Tyr334, His440 while the amino acid residues Tyr70, Val71, Asp72, Gly117, Gly118, Tyr121, Ser122, Gly123, Phe330, Leu333, Tyr334, Trp432, Met436, Ile439, His440, Tyr442 were engaged in van der Waals interactions, and the amino acid residues Tyr70, Trp84, Phe330, Phe331, Tyr334, Trp432 and His440 were involved in π–π stacking interactions (Table 2; Figure 4). Further, with hBChE, compounds **15-28** formed hydrogen bonds to the amino acids Tyr82, Tyr128, Tyr332, Tyr449, His438 and involved in van der Waals interactions to residues side chains of Asp70, Trp82, Gly116, Gly117, Gly119, Tyr120, Gly121, Ser196, Glu197, Ser198, Trp231, Leu286, Ser287, Ala328, Phe329, Tyr332, Trp430 while the amino acid residues Trp82, Tyr128, Ala328, Phe329, Tyr332, Phe398, Trp430, His438, Tyr440 were engaged in Pi–Pi interactions (Table 7; Figure 4a,b).

Table 2. Experimental and predicted BACE1 inhibition % and docking results of (10 μmol) compounds **15-28**.

No.	Binding Energy Kcalmol^{-1}	Inhibition constant (Ki nmol)	Exp. inhibition %	Binding residues	Hydrogen bonds (distance, Å)
15	-12.54	0.638	83.4	Leu30, Asp32, Tyr71, Gln73, Lys107, Ile110, Trp115, Asp228, Thr231, Thr320	Phe108
16	-13.16	0.227	87.0	Gln12, Gly13, Leu30, Asp32, Tyr71, Gln73, Lys107, Phe108, Asp228,Gly230, Thr231, Thr282	Thr72
17	-12.86	0.376	63.1	Gln12, Gly13, Leu30, Asp32, Tyr71, Gln73, Lys107, Phe108, Asp228,Gly230, Arg235, Thr282	Thr72
18	-13.65	0.099	74.5	Gln12, Gly13, Leu30, Asp32, Tyr71, Gln73, Lys107, Phe108, Asp228,Gly230, Thr231, Thr282	Thr72
19	-13.62	0.103	72.1	Gln12, Gly13, Leu30, Asp32, Tyr71, Gln73, Lys107, Phe108, Asp228,Gly230, Thr231, Thr282	Thr72
20	-13.19	0.213	62.4	Gly13, Asp32, Tyr71, Gln73, Gly74, Lys107, Phe108, Asp228,Gly230, Thr231, Thr282	Thr72
21	-11.32	5.02	60.5	Gln12, Gly13, Tyr71, Gln73, Gly230, Thr231, Thr282	Thr72
22	-12.05	1.47	61.9	Leu30, Tyr71,Thr72, Gln73, Lys107, Ile110, Trp115, Gly230, Thr231, Arg235	Phe108
23	-11.33	4.9	79.7	Gln12, Gly13, Leu30, Tyr71, Gln73, Asp228, Gly230, Thr231, Arg235, Val232	Thr72
24	-10.12	38.3	89.2	Gln12, Gly13, Tyr71, Gln73, Lys107, Phe108, Asp228,Gly230, Thr231, Thr282	Thr72

 doi:10.20944/preprints202402.0731.v1

25	-11.82	2.16	83.1	Leu30, Tyr71,Thr72, Gln73, Ile110, Ile118, Asp228, Thr229, Gly230, Thr231, Thr232	Phe108
26	-12.51	0.681	91.0	Gln12, Gly13, Leu30, Tyr71, Thr72, Gln73, Phe108, Ile110, Trp115, Asp228,Gly230, Thr231, Arg235	Lys107
27	-12.59	0.593	81.3	Gly13, Asp32, Tyr71, Gln73, Phe108, Ile110, Ile226, Asp228,Gly230, Thr231,Thr232,Arg235, Val332, Thr329	Lys107
28	-9.98	56.95	78.6	Tyr71, Lys107, Phe108, Ile110, Asp228,Thr229, Thr231, Arg235, Val332	----
Xray	-11.45	4.0	nd	Leu30, Asp32, Tyr71, Lys107, Phe108, Ile110, Trp115,Asp228,Thr229, Gly230, Arg235	Gln73, Phe108, Asp228

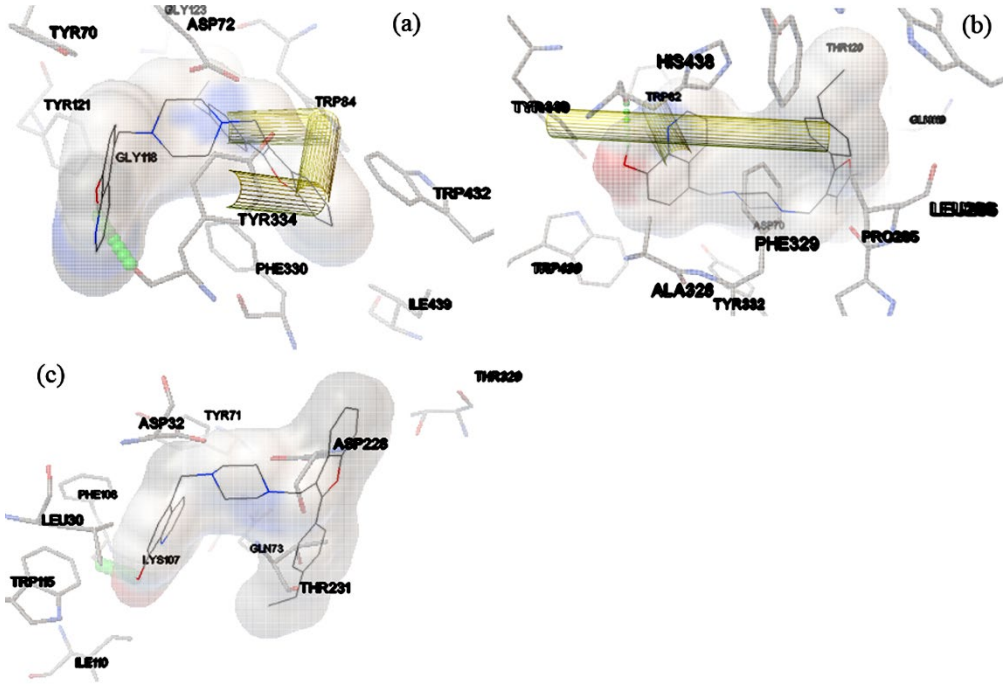

Figure 4. Compound **15** to the binding site of tcAChE (5nnu.pdb) (a), hBChE structure (6i0b.pdb) (b) and binding site of BACE1 structure (4ivt.pdb) (c).

Table 3. Docking study results of compounds **15-28** to AChE and BChE.

No	Binding residues		Hydrogen bonds (distance, Å)		Pi-pi interactions	
	AChE	BChE	AChE	BChE	AChE	BChE
15	Tyr70,Asp72,Gly118, Tyr121, Gly123, Phe330, Tyr334, Trp432, Ile439	Asp70,Trp82,Gln119, Tyr120,Pro285,Leu286, Ala328,Phe329,Tyr332, Trp429	Tyr334	His438	Trp84, Tyr334	Tyr440
16	Tyr70,Asp72,Gly118, Tyr121, Ser122, Phe330, Leu333, Trp432, Met436	Asp70,Gly116, Gln119, Ser196,Pro285, Ser287, Asn289, Ala328, Phe329, Tyr332	Tyr334	His438	Trp84	Trp82, Tyr440
17	Asp72, Gly118, Tyr121, Ser122, Gly123, Phe330	Gly115,Gly117,Gln119, Gly121,Glu197,Ser198, Trp231, Pro285,Leu286, Ser287,Phe329, Phe398	Tyr334	His438	Tyr70, Trp84, Trp432	Trp82, Phe329, Phe398
18	Tyr70, Asp72, Gly118, Tyr121, Ser122, Trp432, Met436	Tpr82, Gly115,Gly117, Gln119,Ser198, Pro285, Leu286,Ser287, Ala328	Tyr334	His438	Trp84, Phe330	Tyr332
19	Tyr70,Asp72,Gly118, Tyr121, Ser122, Phe330, Trp432, Met436	Asp70,Gly117, Leu286, Ala328,Phe329,Tyr332, Trp430, Tyr440	Tyr334	His438	Trp84	Trp82, His438

 doi:10.20944/preprints202402.0731.v1

20	Tyr70,Asp72,Gly117, Gly118, Phe330, Trp432, Met436, Ile439, His440, Tyr442	Gly115, Gly117, Gln119, Pro285, Ser287, Ala328 Tyr332, Trp430, Tyr440	Tyr334	His438	Trp84	Trp82, Tyr440
21	Tyr70,Asp72, Asn85, Pro86,Gln89,Tyr121, Tyr334, Phe330, Tyr442, Ile439	Gly116, Thr120, Glu197, Pro285, Ala328, Phe329, Tyr332, Trp430	His440	His438	Trp84, Phe330, His440	Trp82, Tyr128, Tyr332
22	Asp72, Gly118, Tyr121, Phe290, Tyr334, Trp432, Ile439	Gly117, Thr120, Trp231, Leu286, Phe398	His440	His438	Trp84, Phe330, His440	Trp82, Ala328
23	Tyr70, Val71, Asp72, Asn85, Tyr121, Ser122, Trp279, Phe331, Tyr334, His440, Gly441	Asp70, Trp82, Gly115, Gly116, THR120, Tyr128, Pro285, Leu286, Ala328, Tyr332, Trp430	Tyr334	His438	Trp84	Tyr440
24	Asp72, Gly118, Tyr121, Ser122, Leu127, Trp279, Trp432, Ile439	Gly115, Gly116, Gly117, Gln119, Tyr128, Ser198, Pro285, Ala328, Phe329, Tyr332, Trp430, Tyr440	Tyr334	His438	Trp84, Phe330	Trp82, Trp430, Tyr440
25	Asp72, Ser81, Trp84, Gly118, Gly119, Tyr121, Phe290, Phe330, Phe331, Trp432	Gly117, Thr120, Trp198, Leu286, Ala328, Tyr332, Phe398, Trp430, Tyr440	Tyr334	His438	Phe330	Trp82, His438, Tyr440
26	Val71, Asp72, Gly118, Gly119, Tyr121, Trp279, Phe290, Phe330,Tyr334, His440	Asp70, Trp82, Gly116, THR120, Glu197, Ser198, Pro285, Ala328,Tyr332, Trp430	Ser122	His438	Tyr70	His438
27	Asp72, Trp84, Gly118, Tyr121, Ser122, Trp279, Phe290, Phe330,Phe331,Tyr334, Gly335, His440	Gly115, Gly116, THR120, Glu197, Ser198, Ser287, Ala328, Phe329, His438	Tyr70	Trp82	Phe331	Tyr332, Tyr440
28	Tyr70, Asp72, Trp84, Asn85,Gly118,Tyr121, Ser122, Trp279, Tyr334	Gly116, Ser198, Thr284, Pro285, Ala328, Tyr332, Tyr440	His440	His438	Phe330	Trp82, Tyr440
Xray	Tyr70, Asp72, Tyr121, Trp279, Phe330, Tyr334, Gly335, Trp432, Met436, Ile439, His440, Gly441,	Asp70, Gly115,Gln119, Ser196, Glu197 Ser198, Pro285,Leu286,Ala328, Phe329, Trp430, Met437, Tyr440	Tyr121	His438	Trp84	Ala328, Tyr440

2.4. Docking study of compounds 15-28 against BAC1 enzyme structures

Using Autodock4.0, we were able to ascertain the molecular interactions and binding affinities between compounds **15–28** and BACE1. The crystal structure of BACE1 (4ivt) [28] was first obtained from the protein database PDB. Before being docked to the macromolecule structure, the compounds **15–28** were sketched, optimized, and uploaded to pdbqt format. The results of the docking investigation were consistent with the experimental BACE1 inhibition values. The early assessment of binding energies based on the docking data revealed the efficiency of the complex system (Table 2), binding locations, and interacting residues with the binders **15–28** (Table 2, Figure 4c). For the complexes of compounds **15-28** with BACE1, docking study has estimated the energy of binding in the energy-value range -13.65 to -9.98 kcal mol^{-1} and revealed the major contributions of the hydrogen bonds and hydrophobic interactions. The docked poses inside the binding site showed the hydrogen-bonding to Thr72, Phe108, Lys107 and van der Waal interactions to hydrophobic side chains of the residues Gln12, Gly13, Leu30, Leu30, Asp32, Tyr71,Thr72, Gln73, Lys107, Phe108, Ile110, Trp115, Gly230, Thr231, Arg235 that is (Table 2, Figure 4c).

2.5. Molecular Dynamics Simulations

The simulation approach allowed the observation of how binders' conformations changed within the macromolecule's binding region. By comparing the RMSD values of the resultant conformations to the starting structure, the dynamic stabilities of the complex system was investigated.

Using Amber tools22 [29] compounds **22, 18** and **26** structural alterations were discovered during the simulation period of their complexes with 5nuu, 6i0b and 4ivt respectively. The difference between the final and the initial protein-ligand coordinates was calculated using Root Mean Square Deviation (RMSD). The stability of the system was measured by the divergence from the original conformation that took place during the simulation. Less variations result from more stable structures.

 doi:10.20944/preprints202402.0731.v1

A root mean square fluctuation (RMSF) study can be used to determine which parts of the protein-ligand complex are more flexible. In Figure 5, the RMSF was shown through the final 4 ns. We looked at how flexibility evolved over MD simulations in order to pinpoint some significant trends for the protein-binder complex system. For the average flexibility of each residue in the macromolecule peptides, 5nuu-compound 22, 6i0b-compound 18, and 4ivt-compound 26, the RMSF at the C-α of each amino acid residue was taken into account and the areas with the greatest fluctuations during the simulation are shown by peaks.

The amino acids that has low values of rmsf are less mobile and stabilized by the hydrogen bond or hydrophobic interaction with the binder ligand. For tcAChE the residues are Tyr76, Val68, Asp69, Ser78, Trp81, Asn82, Tyr118, Ser119, Glu196, Trp276, Ile284, Phe287, Phe327, Phe328, Tyr331, Trp429, Ile436, His437, Tyr439. For hBChE the residues are Leu107, Ile108, Trp109, Ile110, Tyr111, Phe115, Gln116, Thr117, Glu194, Ser195, Ala196, Ala199, Tyr393, Asn394, Phe395, Ile396, Met435, His435, Tyr437, Glu438, Ile439. For BACE1 the residues are Gln12, Leu30, Tyr71, Thr72, Gln73, Lys107, Phe108, Ile110, Trp115, Thr231, Thr232, Asn233, Ser325, Gln326, Ser327, Thr329, Ile386,

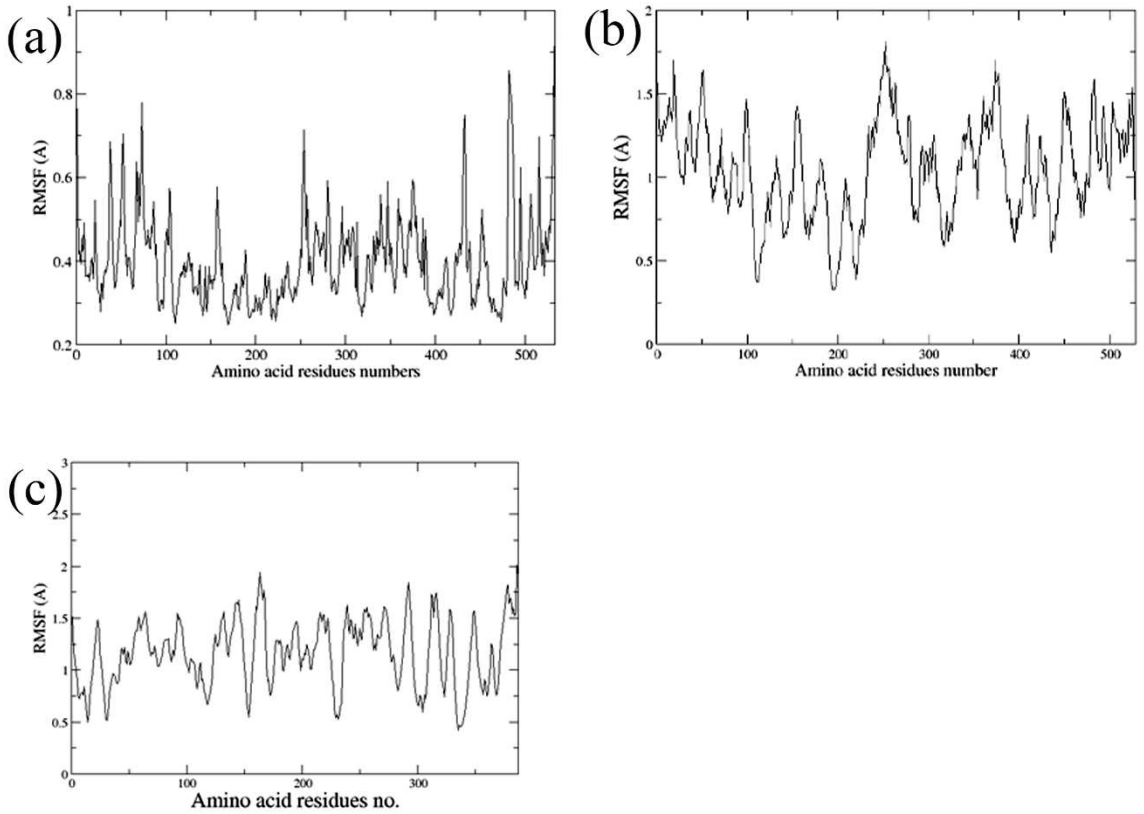

Figure 5. The RMSF chart of amino acid residues of 5nuu-compoud 22 (a), 6i0b-compound 18 (b) and 4ivt-compound 26 (c) complexes during simulation process..

Figure 6. shows the average structure for the 5nnu-22, 6i0b-18 and 4ivt-26 generated from the last 4 ns trajectory data of the MD simulations process. The van der Waals interaction energy has a major contributions to the total binding more than the electrostatic contributions. This suggest the crucial role of the hydrophobic residues delineating the binding sites of tcAChE, hBChE and BACE1 protein structure.

Preprints.org (www.preprints.org) | NOT PEER-REVIEWED | Posted: 13 February 2024 doi:10.20944/preprints202402.0731.v1

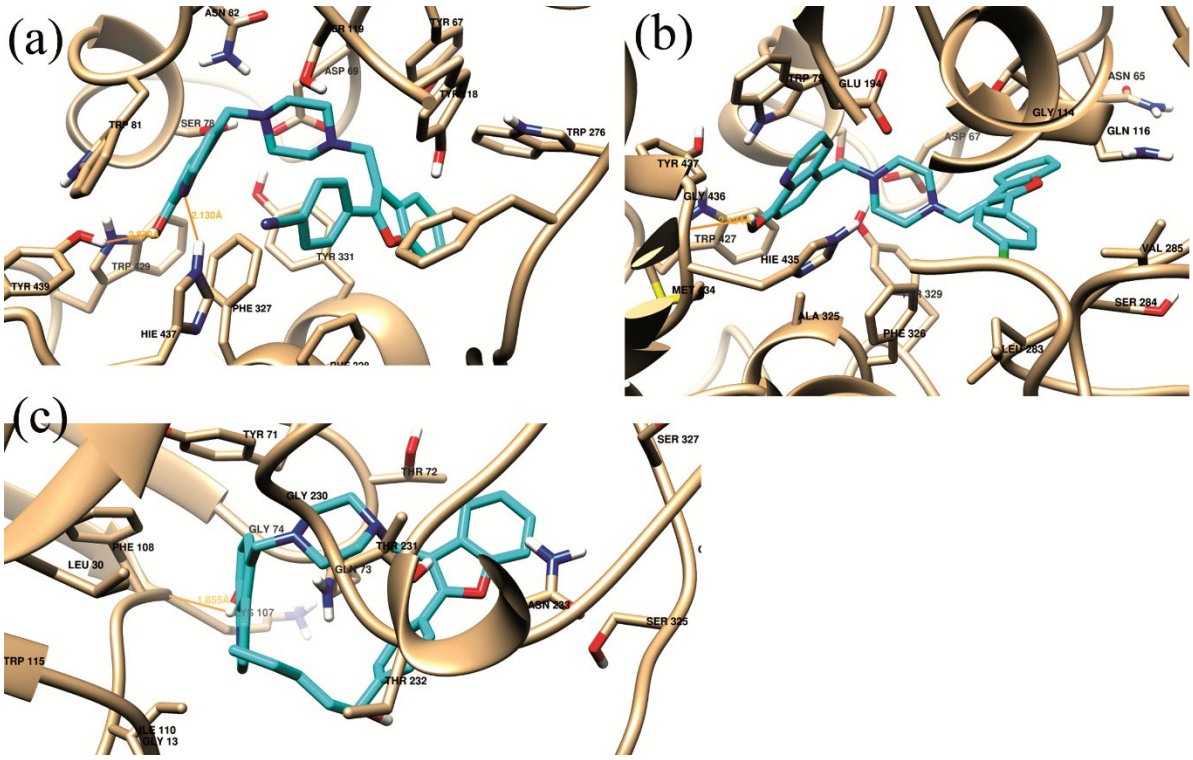

Figure 6. The averaged 5nuu-compoud 22 (a), 6i0b-compound 18 (b) and 4ivt-compound 26 (c)-structures of tcAChE, hBChE and BACE1 complexes. The hydrogen bonds (orange solid lines); Amino acids (beige-colored sticks); The ligand (a cyan-colored stick).

Table 4 shows the MM/GBSA total binding energy of 5nuu-compoud **22** (-57.0944 kcal mol^{-1}), 6i0b-compound **18** (-51.7731 kcal mol^{-1}) and 4ivt-compound **26** (c) (-42.8924 kcal mol^{-1}). In the three complex systems, 5nnu -**22**, 6i0b-**18** and 4ivt-**26**, the ligands are anchored inside the binding site through the hydrogen bond of the ligands to Hie437, Hie435 and Lys107 respectively (Table 4). At the same time, the van der Waals interactions of the ligands with the hydrophobic side chains of the surrounding amino acid residues support the bound conformations as explored by MM/PBSA pairwise decomposition analysis (Table 5). The residues Hie437, Trp79 and Tyr71 have major contributions to the ligand protein interaction energies of 5nnu, 6i0b and 4ivt respectively.

Table 4. The MM/GBSA binding free energy (kcal mol^{-1}) of 5nuu-compoud 22 (a), 6i0b-compound 18 (b) and 4ivt-compound 26 (c) of tcAChE, hBChE and BACE1 complexes.

Complex	Hb-residue (Frac %)	ΔG_{vdw}	ΔG_{elec}	ΔG_{polar}[a]	ΔG_{Surf} [b]	$\Delta G_{MM/GBSA}$
(a)	HIE_437@HE2(16.25%) SER_197@HG (11.5%)	-67.9357	-18.8145	36.9524	-7.2966	-57.0944
(b)	HIE_435@O (42.25%) THR_231@HB (10.25%)	-60.6058	-8.3630	23.8192	-6.6235	-51.7731
(c)	THR_232@H (9.5%) LYS_107@O (33.75%)	-49.274	-6.0429	18.5027	-6.0780	-42.8924

a ΔGelectrostatic + ΔGpolar are the whole electorstatic contribution. b ΔGnp = ΔGvdw + ΔGsurf are the whole non polar contribution.

 doi:10.20944/preprints202402.0731.v1

Table 5. The results of MM/PBSA-pairwise-residue decomposition analysis of 5nuu-compoud 22 (a), 6i0b-compound 18 (b) and 4ivt-compound 26 (c) complexes.

Complex	Residue Number Residue interaction energy kcalmol^{-1}									
(a)	Asp69	Ser78	Trp81	Asn82	Tyr118	Phe327	Phe328	Tyr331	Hie437	Tyr439
	-2.425	-2.294	-3.357	-1.732	-2.301	-2.227	-2.342	-3.312	-4.539	-1.749
(b)	Asp67	Trp79	Gln116	Thr117	Glu194	Ala325	Phe326	Tyr329	Met434	Hie435
	-1.703	-3.81	-2.185	-1.58	-1.538	-1.947	-1.613	-1.768	-1.21	-2.594
(c)	Gln12	Tyr71	Thr72	Gln73	Lys107	Phe108	Ile110	Gly230	Thr231	Thr232
	-1.046	-3.218	-1.382	-5.179	-1.412	-2.287	-0.864	-1.344	-2.098	-1.408

3. Experiment and procedures

3.1. Chemistry

The starting materials and reagents were purchased from Sigma-Aldrich (St. Louis, MO, USA). Without any adjustments, the melting points were calculated using a Stuart Scientific electrothermal melting point equipment from Stone, Staffordshire, UK. Thin layer chromatography (TLC) was performed using precoated silica gel plates (0.25 mm, 60G F254, Merck, Darmstadt, Germany) and a chloroform/methanol (8:2) developing solution. The chemical structure spectrum study was finished at the research center of King Saud University College of Pharmacy. An FTIR spectrophotometer was used to capture IR spectra on KBr plates. Shelton, Connecticut, USA: Perkin Elmer. An NMR spectrophotometer (Bruker, Flawil, Switzerland) that operates at 500 MHz for ^{1}H and 125.76 MHz for ^{13}C was used to produce nuclear magnetic resonance (NMR) spectra. Mass spectra were collected using a model 320 MS spectrometer. USA (Varian, Lexington, KY). A Perkin Elmer model 2400 elemental analyser was used to examine the elements. The intermediate compounds 5-chloromethyl-8-hydroxyquinoline hydrochloride **3**, 5-chloromethyl-8-hydroxyquinoline hydrochloride **5** and the final compounds 5-((4-((2-(4-substitutedphenyl)benzofuran-3-yl)methyl)piperazin-1-yl)methyl)quinolin-8-ol derivatives **15-21** were prepare as reported [22, 24].

5-((4-((2-(4-Ethylphenyl)benzofuran-3-yl)methyl)piperazin-1-yl)methyl)quinolin-8-ol (**15**): White solid, yield 85%, mp 100–101 °C [24].

5-((4-((2-(4-Methoxyphenyl)benzofuran-3-yl)methyl)piperazin-1-yl)methyl)quinolin-8-ol (**16**): White solid, yield 80%, mp 141–142 °C [24].

5-((4-((2-(4-Fluorophenyl)benzofuran-3-yl)methyl)piperazin-1-yl)methyl)quinolin-8-ol (**17**): White solid, yield 75%, mp 118–119 °C [24].

5-((4-((2-(4-Chlorophenyl)benzofuran-3-yl)methyl)piperazin-1-yl)methyl)quinolin-8-ol (**18**): White solid, yield 90%, mp 134–135 °C [24].

5-((4-((2-(4-Bromophenyl)benzofuran-3-yl)methyl)piperazin-1-yl)methyl)quinolin-8-ol (**19**): Beige solid, yield 70%, mp 115–116 °C [24].

5-((4-((2-p-Tolylbenzofuran-3-yl)methyl)piperazin-1-yl)methyl)quinolin-8-ol (**20**): White solid, yield 78%, mp 116–117 °C [24].

5-((4-((2-Biphenylbenzofuran-3-yl)methyl)piperazin-1-yl)methyl)quinolin-8-ol (**21**): White solid, yield 65%, mp 206–207 °C [24].

3.1.1. General synthesis of 2-(4-substitutedphenyl)benzofuran derivatives (8-14)

2-hydroxybenzyltriphenyl phosphonium bromide (12 g, 27 mmol), 4-substitutedbenzoylchloride (5 g, 29 mmol) in presence of triethylamine (11.1 mL, 80 mmol) were combined and refluxed for 10 hours in toluene (125 mL). The reaction mixture was concentrated under reduced pressure into greasy residue that received 120 mL of ethanol before being chilled overnight. The resulting solid underwent filtering, drying, and recrystallization from ethanol.

 doi:10.20944/preprints202402.0731.v1

4-(Benzofuran-2-yl)benzonitrile (**8**); White solid, mp 205-6 °C 3048 (arom CH str), 2220 (CN str), 881-691 (arom CH bend). ^{1}H NMR (700 MHz, $CDCl_3$): δ = 7.19-8.21 (9H, m, ArH). ^{13}CNMR (100 MHz, $CDCl_3$): δ = 101.54, 111.43, 112.85, 115.97, 120.92, 122.95, 123.32, 124.76, 127.81, 132.84, 133.91, 154.87, 156.02. Ms m/z calcd: 219.07 $[M]^+$, found: 219.48 $[M]^+$. Anal. calcd. for $C_{15}H_9NO$: C, 82.18; H, 4.14; N, 6.39. Found: C, 82.32; H, 4.21; N, 6.26.

2-(4-(*tri*Fluoromethyl)phenyl)benzofuran (**9**); White solid, mp 156-7 °C 3044 (arom CH str), 799-706 (arom CH bend). ^{1}H NMR (700 MHz, $CDCl_3$): δ = 7.16-8.00 (9H, m, ArH). ^{13}CNMR (100 MHz, $CDCl_3$): δ = 102.05, 111.22, 118.11, 122.45, 123.92, 123.95, 124.55, 125.15, 128.12, 130.72, 134.05, 154.83, 156.65. Ms m/z calcd: 262.06 $[M]^+$, found: 262.38 $[M]^+$. Anal. calcd. for $C_{15}H_9F_3O$: C, 68.70; H, 3.46. Found: C, 68.55; H, 3.62.

2-(4-Butylphenyl)benzofuran (**10**); White solid, mp 133-4 °C 3055 (arom CH str), 847-696 (arom CH bend). ^{1}H NMR (700 MHz, $CDCl_3$): δ = 0.93 (3H, t, CH_3), 1.25-1.38 (2H, m, CH_2), 1.60-1.65 (2H, m, CH_2), 2.66 (2H, t, CH_2), 6.72-7.69 (9H, m, ArH). ^{13}CNMR (100 MHz, $CDCl_3$): δ = 14.35, 21.32, 31.89, 36.47, 101.83, 110.46, 119.79, 122.95, 123.47, 123.95, 126.55, 127.15, 128.12, 137.22, 153.94, 155.38. Ms m/z calcd: 250.14 $[M]^+$, found: 250.62 $[M]^+$. Anal. calcd. for $C_{18}H_{18}O$: C, 86.36; H, 7.25. Found: C, 86.48; H, 7.16.

2-(4-*tert*-Butylphenyl)benzofuran (**11**); White solid, mp 118-9 °C 3042 (arom CH str), 799-706 (arom CH bend). ^{1}H NMR (700 MHz, $CDCl_3$): δ = 1.32 (9H, t, three CH_3), 6.71-7.86 (9H, m, ArH). ^{13}CNMR (100 MHz, $CDCl_3$): δ = 31.68, 34.78, 100.69, 111.13, 120.77, 122.68, 123.47, 123.34, 124.56, 125.75, 127.74, 151.81, 154.83, 156.37. Ms m/z calcd: 250.14 $[M]^+$, found: 250.39 $[M]^+$. Anal. calcd. for $C_{18}H_{18}O$: C, 86.36; H, 7.25. Found: C, 86.24; H, 7.39.

2-(4-Pentylphenyl)benzofuran (**12**); White solid, mp 116-7 °C 3045 (arom CH str), 829-706 (arom CH bend). ^{1}H NMR (700 MHz, $CDCl_3$): δ = 0.85 (3H, t, CH_3), 1.22-1.30 (4H, m, two CH_2), 1.60-1.65 (2H, m, CH_2), 2.66 (2H, t, CH_2), 6.92-7.81 (9H, m, ArH). ^{13}CNMR (100 MHz, $CDCl_3$): δ = 14.38, 22.40, 30.72, 31.34, 35.52, 102.10, 111.47, 121.44, 122.12, 123.02, 125.13, 126.15, 127.15, 128.02, 138.04, 154.36, 156.65. Ms m/z calcd: 264.15 $[M]^+$, found: 264.47 $[M]^+$. Anal. calcd. for $C_{19}H_{20}O$: C, 86.32; H, 7.63. Found: C, 86.46; H, 7.52.

2-(4-Hexylphenyl)benzofuran (**13**); White solid, mp 114-5 C 3044 (arom CH str), 799-706 (arom CH bend). ^{1}H NMR (700 MHz, $CDCl_3$): δ = 0.89 (3H, t, CH_3), 1.24-1.42 (6H, m, three CH_2), 1.56-1.67 (2H, m, CH_2), 2.58 (2H, t, CH_2), 6.68-7.82 (9H, m, ArH). ^{13}CNMR (100 MHz, $CDCl_3$): δ = 14.23, 22.71, 28.83, 30.88, 31.12, 35.84, 102.25, 111.61, 121.01, 123.05, 123.48, 124.11, 127.04, 127.72, 128.11, 138.33, 155.01, 156.48 Ms m/z calcd: 278.17 $[M]^+$, found: 278.59 $[M]^+$. Anal. calcd. for $C_{20}H_{22}O$: C, 86.29; H, 7.97. Found: C, 86.15; H, 8.13.

2-(Thiophen-2-yl)benzofuran **(14);** White solid, mp 186-7 °C 3041 (arom CH str), 829-707 (arom CH bend). ^{1}H NMR (700 MHz, $CDCl_3$): δ = 6.72-7.70 (9H, m, ArH). ^{13}CNMR (100 MHz, $CDCl_3$): δ = 102.08, 111.22, 121.36, 123.11, 123.76, 124.05, 125.04, 126.13, 127.15, 132.73, 155.25, 156.11 Ms m/z calcd: 200.03 $[M]^+$, found: 200.46 $[M]^+$. Anal. calcd. for $C_{12}H_8OS$: C, 71.97; H, 4.03; S, 16.01. Found: C, 71.82; H, 3.91; S, 16.25.

3.1.2. General synthesis of 5-((4-((2-(4-substitutedphenyl)benzofuran-3-yl)methyl)piperazin-1-yl)methyl)quinolin-8-ol derivatives (22-28)

To a DMF (10 mL) solution of 2-(4-Substitutedphenyl)benzofuran (**8-14**) (10 mmol), formaline (37%, 1.55 mL) and 5-((piperazin-1-yl)methyl)quinolin-8-ol (10 mmol) were added and stirred at r.t. for 3 h. Excess water was added to the reaction mixture and allowed to 24 h in cold. The purified precipitate was obtained after filtering, water washing, and recrystallization from ethanol.

4-(3-((4-((8-Hydroxyquinolin-5-yl)methyl)piperazin-1-yl)methyl)benzofuran-2-yl)benzonitrile (**22**) White solid, yield 70%, mp 177-8 °C. IR (λmax, cm^{-1}): 3403 (OH str), 3050 (arom CH str), 2930 (aliph CH str), 2222 (CN str), 887-710 (arom CH bend). 1H NMR (700 MHz, $CDCl_3$): δ = 2.9 (4H, s, $2CH_2$), 2.97 (4H, s, $2CH_2$), 3.75 (2H, s, CH_2), 3.76 (2H, s, CH_2), 7.02-8.63 (13H, m, ArH). 13CNMR (100 MHz, DMSO-d_6): δ = 41.05, 51.83, 52.01, 57.54, 110.74, 112.08, 113.11, 114.56, 117.39, 120.72, 121.33, 123.22, 123.88, 124.05, 125.91, 126.24, 128.12, 128.52, 132.02, 132.35, 133.95, 136.73, 148.56, 151.40,

 doi:10.20944/preprints202402.0731.v1

151.64, 155.52. Ms m/z calcd: 474.21 $[M]^+$, found 474.58 $[M]^+$. Anal. calcd. for $C_{30}H_{26}N_4O_2$: C, 75.93; H, 5.52; N, 11.81. Found: C, 75.78; H, 5.41; N, 11.97.

5-((4-((2-(4-(*tri*Fluoromethyl)phenyl)benzofuran-3-yl)methyl)piperazin-1-yl)methyl)quinolin-8-ol **(23)** White solid, yield 65%, mp 133-4 °C. IR (λmax, cm^{-1}): 3403 (OH str), 3048 (arom CH str), 2955 (aliph CH str), 837-660 (arom CH bend). 1H NMR (700 MHz, $CDCl_3$): δ = 2.91 (4H, s, $2CH_2$), 2.98 (4H, s, $2CH_2$), 3.76 (2H, s, CH_2), 3.78 (2H, s, CH_2), 6.99-8.54 (13H, m, ArH). 13CNMR (100 MHz, DMSO-d_6): δ = 41.72, 52.04, 52.42, 58.33, 111.12, 112.63, 113.05, 117.11, 120.81, 121.14, 123.45, 123.05, 124.66, 125.12, 126.01, 126.78, 127.34, 127.95, 130.38, 131.25, 132.73, 138.16, 149.41, 150.64, 151.48, 156.33. Ms m/z calcd: 517.2 $[M]^+$, found 517.58 $[M]^+$. Anal. calcd. for $C_{30}H_{26}F_3N_3O_2$. C, 69.62; H, 5.06; N, 8.12. Found: C, 69.73; H, 4.91; N, 8.05.

5-((4-((2-(4-Butylphenyl)benzofuran-3-yl)methyl)piperazin-1-yl)methyl)quinolin-8-ol **(24)** White solid, yield 65%, mp 171-2 °C. IR (λmax, cm^{-1}): 3358 (OH str), 3042 (arom CH str), 2917 (aliph CH str), 796-739 (arom CH bend). 1H NMR (700 MHz, $CDCl_3$): δ = 0.98 (3H, t, CH_3), 1.39-1.45 (2H, m, CH_2), 1.63-1.69 (2H, m, CH_2), 2.67-2.70 (10H,m, four piperazine-CH_2 and -CH_2-), 3.76 (2H, s, CH_2), 3.79 (2H, s, CH_2), 7.0-8.48 (13H, m, ArH). 13CNMR (100 MHz, DMSO-d_6): δ = 14.21, 22.08, 32.78, 36.11, 41.33, 51.82, 52.62, 57.87, 110.59, 112.77, 117.05, 120.81, 121.53, 123.14, 124.03, 124.26, 125.66, 126.11, 127.01, 127.22, 128.34, 128.47, 130.92, 137.55, 138.48, 148.74, 151.41, 151.29, 154.08. Ms m/z calcd: 505.27 $[M]^+$, found 505.78 $[M]^+$. Anal. calcd. for $C_{33}H_{35}N_3O_2$: C, 78.38; H, 6.98; N, 8.31. Found: C, 78.22; H, 6.81; N, 8.45.

5-((4-((2-(4-*tert*-Butylphenyl)benzofuran-3-yl)methyl)piperazin-1-yl)methyl)quinolin-8-ol **(25)** White solid, yield 65%, mp 220-C. IR (λmax, cm^{-1}): 3344 (OH str), 3094 (arom CH str), 2912 (aliph CH str), 794-602 (arom CH bend). 1H NMR (700 MHz, $CDCl_3$): δ = 1.39 (9H, s, three CH_3), 2.9 (4H, t, two CH_2), 2.97 (4H, t, two CH_2), 3.72 (2H, s, CH_2), 3.81 (2H, s, CH_2), 7.01-8.61 (13H, m, ArH). 13CNMR (100 MHz, DMSO-d_6): δ = 31.15, 34.78, 36.50, 51.81, 53.57, 57.06, 111.13, 112.9, 117.3, 120.77, 121.16, 123.34, 124.0, 124.56, 125.32, 125.57, 125.89, 126.08, 127.74, 129.37, 131.32, 137.05, 138.48, 151.81, 154.83, 156.17, 156.37, 162.58. Ms m/z calcd: 505.27 $[M]^+$, found 505.78 $[M]^+$. Anal. calcd. for $C_{33}H_{35}N_3O_2$: C, 78.38; H, 6.98; N, 8.31. Found: C, 78.41; H, 7.05; N, 8.24.

5-((4-((2-(4-pentylphenyl)benzofuran-3-yl)methyl)piperazin-1-yl)methyl)quinolin-8-ol **(26)** White solid, yield 65%, mp 198-9 **°C.** IR (λmax, cm^{-1}): 3361 (OH str), 3045 (arom CH str), 2933 (aliph CH str), 798-609 (arom CH bend). 1H NMR (700 MHz, DMSO-d_6): δ = 0.85 (3H, t, CH_3), 1.22-1.30 (4H, m, two CH_2), 1.52-1.60 (3H, m, CH_2), 2.55-2.68 (10H, m, four piperazine-CH_2 and pentyl –CH_2), 3.83 (2H, s, CH_2), 4.29 (2H, s, CH_2), 7.11-8.81 (13H, m, ArH). 13CNMR (100 MHz, DMSO-d_6): δ = 19.01, 25.93, 31.0, 31.15, 37.0, 36.50, 49.05, 56.04, 57.06, 62.49, 110.71, 114.12, 114.91, 120.60, 121.47, 122.16, 127.21, 128.75, 130.03, 133.30, 134.89, 145.24, 153.57, 153.67, 162.01. Ms m/z calcd: 519.29 $[M]^+$, found 519.72 $[M]^+$. Anal. calcd. for $C_{34}H_{37}N_3O_2$: C, 78.58; H, 7.18; N, 8.09. Found: C, 78.42; H, 7.05; N, 8.16.

5-((4-((2-(4-hexylphenyl)benzofuran-3-yl)methyl)piperazin-1-yl)methyl)quinolin-8-ol **(27)** White solid, yield 65%, mp 186-7 **°C.** IR (λmax, cm^{-1}): 3358 (OH str), 3077 (arom CH str), 2927 (aliph CH str), 823-745 (arom CH bend). 1H NMR (700 MHz, $CDCl_3$): δ = 0.81 (3H, t, CH_3), 1.24-1.29 (6H, m, three CH_2), 1.53-1.59 (3H, m, CH_2), 2.55-2.59 (2H, t, CH_2), 2.80 (4H, t, two CH_2), 2.88 (4H, t, two CH_2), 3.66 (2H, s, CH_2), 3.69 (2H, s, CH_2), 6.90-8.78 (13H, m, ArH). 13CNMR (100 MHz, $CDCl_3$): δ = 15.11, 21.45, 29.23, 31.5, 31.56, 36.61, 38.88, 51.05, 52.34, 58.04, 111.08, 113.27, 117.05, 120.84, 121.16, 122.78, 124.25, 124.95, 125.05, 126.44, 127.01, 127.15, 127.46, 128.11, 128.43, 130.85, 137.12, 138.55, 150.05, 151.12, 151.35, 154.28. Ms m/z calcd: 533.3 $[M]^+$, found 533.69 $[M]^+$. Anal. calcd. for $C_{35}H_{39}N_3O_2$: C, 78.77; H, 7.37; N, 7.87. Found: C, 78.64; H, 7.21; N, 7.93.

5-((4-((2-(Thiophen-2-yl)benzofuran-3-yl)methyl)piperazin-1-yl)methyl)quinolin-8-ol **(28)** White solid, yield 65%, mp 225-6 **°C.** IR (λmax, cm^{-1}): 3361 (OH str), 3055 (arom CH str), 2928 (aliph CH str), 819-709 (arom CH bend). 1H NMR (700 MHz, $CDCl_3$): δ = 2.9 (4H, t, two CH_2), 2.97 (4H, t, two CH_2), 3.51 (2H, s, CH_2), 3.75 (2H, s, CH_2), 6.89-8.87 (13H, m, ArH). 13CNMR (100 MHz, DMSO-d_6): δ = 51.15, 52.38, 40.18, 57.77, 111.22, 112.56, 117.68, 121.22, 121.73, 123.16, 124.05, 124.71, 125.11, 126.57, 126.89, 127.08, 127.45, 129.15, 131.42, 134.05, 138.17, 149.81, 150.82, 151.22, 154.69. Ms m/z calcd: 455.17 $[M]^+$, found 455.78 $[M]^+$. Anal. calcd. for $C_{27}H_{25}N_3O_2S$: C, 71.18; H, 5.53; N, 9.22; S, 7.04. Found: C, 71.04; H, 5.42; N, 9.11; S, 7.18.

 doi:10.20944/preprints202402.0731.v1

3.2. AChE/BChE screening experiment.

The screening kits for human acety/butyrylcholinesterase inhibitors (ab283363 and ab241010) were bought from abcam in the UK. Using a modified-Ellman's approach, the inhibitory activity of compounds **15–28** against AChE and BuChE were assessed. Stock solutions of the compounds **15–28** (10 μM) were made in ethanol and then diluted further using 0.1 M KH_2PO_4/K_2HPO_4 buffer (pH 8.0), resulting in a final concentration of (0.01-10 μM). The enzyme powder was dissolved in distilled water to create enzyme stock solutions. The assay combination contained 100 mL of various doses of compounds **15–28** along with 1 mL of phosphate buffer (0.1 M, KH_2PO_4/K_2HPO_4), 25 mL of AChE (0.22 U/mL, E.C. 3.1.1.7), or 25 mL of BuChE (0.06 U/mL, E.C. 3.1.1.8). In brief, after 30 minutes of incubation at 37 °C, 20 μL of 10 mmol (acetylthiocholine/butylthiocholine), 10 μL of various chemical concentrations, 10 μL of 0.22 U AChE/BChE, 40 μL of 0.02 mol/phosphate buffer (pH 7.4), and 20 μL of 4% SDS were added to a 96-well microplate to halt the reaction. To create the colour, 100 μL of DTNB was then added.

As a positive control, donepzil (the reference medication) was applied in the same concentration range. 20 mL of the 0.075 M substrate solution (acetylthiocholine/butyrylthiocholine) were added to start the reaction. At 25 °C and 412 nm, the absorbance was measured 2 minutes after the substrate was introduced. In enzyme-free assay techniques, the non-enzymatic hydrolysis of acetylthiocholine/butyrylthiocholine iodide was also considered, and the outcome was utilized as a blank [27]. Then, after subtracting the corresponding background, the absorbances for AChE in the presence and absence of the inhibitors, respectively, were calculated using the formula (1 − Ai / Ac) 100. Each experiment was run in triplicate, and the findings are shown as the mean standard deviation. Whereas Ac denotes absorbance brought on by the intact cholinesterase solution in the absence of AChE inhibitors, Ai denotes absorbance supplied by the cholinesterase solution in the presence of AChE inhibitors.

3.3. BACE-1 Screening Experiment

The BACE1 Inhibitor Screening Kit (Fluorometric) Ab283408 was bought from abcam in the UK. In order to make buffers and standard solutions, purified water was used. Using 96-well plates, spectrofluorometric studies was carried out. A buffer solution of 50 mM sodium acetate and dimethyl sulfoxide was used to dissolve the compounds **15-28** to final concentrations of (0.01-10 μM). The test compounds were treated with 20 μL of BACE-1 (25 nM) for 60 minutes. To the well, was added 20 μL of substrate (0.25 M), and then incubate for 1 hour at 37 °C. The reaction is then slowed down by adding 20 μL of sodium acetate 2.5 M to each well. Then, using a blank devoid of BACE-1, a spectrofluorometric test at 590 nm will be conducted.

3.4. Molecular Docking

The Torpedo California AChE-tacrine complex (TcAChE) (PDB code: 5nnu.pdb), the human BChE complex with ligand (hBChE) (PDB code: 6i0b.pdb), and the complex of BACE1 with the ligand inhibitor (4ivt.pdb) were all X-ray crystallized structures. After removing all water molecules and unnecessary groups. Compound **15** with significant experimental inhibition activity against AChE, BChE and BACE1 enzymes was chosen for molecular docking investigations. The docking studies were performed by Autodock 4.2 software using the Lamarckian genetic method [25]. The nonpolar hydrogen atoms were combined using AutoDock tools and saved in pdbqt format and the polar hydrogen atoms and Kollman charges of the ligands and macromolecule structures were determined. During the docking procedure, the macromolecule structures in the grid box were kept stiff while the ligands were kept flexible. Grid points, 32 x, 32 y, and 32 z, with a spacing of 0.375 Å were defined based on the user-specified number of grid points. The top-ranked ten conformations were produced.

3.5. Molecular Dynamics Simulations

AmberTools22 program was utilized in performing the molecular dynamics simulations using the docked-compounds **22, 18** and **26** to TcAChE (PDB code: 5nnu.pdb), hBChE (PDB code: 6i0b.pdb),

 doi:10.20944/preprints202402.0731.v1

and BACE1 (4ivt.pdb) structures, respectively. The CPPTRAJ module was utilised in analysis of the MD simulations trajectories while the MM/GBSA and MM/PBSA-pairwise decomposition protocols were used to estimate binding free energy and the interaction energy of the macromolecule-residues to the ligands.

4. Conclusions

The work included the synthesis of hybrids of benzofuran and 8-hydroxyquinoline moieties that are linked through piperazine linker. Compounds **15-28** were suggested as potential multimodal anti-AD agents aimed to their superior privilege by their dual ChE (AChE/BChE) and BAC1 inhibitor activities suggesting its potential assignment in cognitive improvement. Compounds 15-28 showed inhibition values 33.4%-81.3% (ACHE), 54.58% - 94.47% (BChE) and 20.9% - 97.9% (BACE1). The experimental results were in accordance with the in silico modeling results and revealed the favorable characteristics of the compounds as promising candidates multi-target inhibitors that could be suggested for further development and studies as potential anti-AD agents. The simulation process declared that Hie437, Hie435 and Lys107 residues are crucial for anchoring and hydrogen bonding to the ligands inside the binding site of tcAChE (5nnu -**22**), hBChE (6i0b-**18**) and BACE1 (4ivt-**26**) respectively. Compounds **22**, **18** and **26** are suggested as lead-compounds for further optimization and studies as inhibitors of tcAChE, hBChE and BACE1 inhibitors respectively.

Author Contributions: Conceptualization: Awwad Radwan, Fars Alanazi. Data curation: Awwad Radwan, Fars Alanazi. Formal analysis: Awwad Radwan, Fars Alanazi. Software: Awwad Radwan, Fars Alanazi. Project administration: Awwad Radwan, Fars Alanazi. Resources: Awwad Radwan. Fars Alanazi. Enzyme Kits assay and analysis of the resulting data, Anas M. Abdel Rahman. Writing –original draft, review & editing: Awwad Radwan, Fars Alanazi.

Funding: This research was funded by the Deanship of Scientific Research, King Saud University, for funding through Vice Deanship of Scientific Research Chairs, Kayyali Chair for Pharmaceutical Industry, Department of Pharmaceutics, College of Pharmacy, for funding the work through Grant Number AW-2023

Data Availability Statement: All the research data are included in the manuscript.

Acknowledgments The authors extend their appreciation to the Deanship of Scientific Research, King Saud University, for funding through Vice Deanship of Scientific Research Chairs, Kayyali Chair for Pharmaceutical Industry, Department of Pharmaceutics, College of Pharmacy, for funding the work through Grant Number AW-2023.

Conflicts of Interest: The authors declare no conflict of interest.

References

1. Yang, H.D.; Kim, D.H.; Lee, S.B.; Young, L.D. History of Alzheimer's disease. Dement. *Neurocogn. Disord*. **2016**, 15, 115-121. doi: 10.12779/dnd.2016.15.4.115.
2. Maramai, S.; Benchekroun, M.; Gabr, M.T.; Yahiaoui, S. Multitarget therapeutic strategies for Alzheimer's disease: Review on emerging target combinations. *BioMed. Res. Int*. **2020**, 5120230. doi: 10.1155/2020/5120230.
3. Iraji, A.; Khoshneviszadeh, M.; Firuzi, O.; Khoshneviszadeh, M.; Edraki, N. Novel small molecule therapeutic agents for Alzheimer disease: focusing on BACE1 and multi-target directed ligands. *Bioorg. Chem*. **2020**, 97, 103649. doi: 10.1016/j.bioorg.2020.103649.
4. Najafi, Z.; Mahdavi, M.; Saeedi, M.; Karimpour-Razkenari, E.; Asatouri, R.; Vafadarnejad, F.; Moghadam, F.H.; Khanavi, M.; Sharifzadeh, M.; Akbarzadeh, T. Novel tacrine-1,2,3-triazole hybrids: in vitro, in vivo biological evaluation and docking study of cholinesterase inhibitors. *Eur. J. Med. Chem.* **2017**, 125, 1200–1212. doi: 10.1016/j.ejmech.2016.11.008.
5. Breijyeh, Z.; Karaman, R. Comprehensive Review on Alzheimer's Disease: Causes and Treatment. *Molecules* **2020**, 25, 5789-5817. doi: 10.3390/molecules25245789.
6. Vafadarnejad, F.; Karimpour-Razkenari, E.; Sameem, B.; Saeedi, M.; Firuzi, O.; Edraki, N.; Mahdavi, M.; Akbarzadeh, T. Novel N-benzylpyridinium moiety linked to arylisoxazole derivatives as selective butyrylcholinesterase inhibitors: synthesis, biological evaluation, and docking study. *Bioorg. Chem*. **2019**, 92, 103192. doi: 10.1016/j.bioorg.2019.103192.

7. Campanari, M.-L.; Navarrete, F.; Ginsberg, S.D.; Manzanares, J.; Sáez-Valero, J., García-Ayllón, M.-S. Increased expression of readthrough acetylcholinesterase variants in the brains of Alzheimer's disease patients. *J. Alzheimers Dis*. **2016**, 53, 831–841. doi: 10.3233/JAD-160220.
8. Darvesh, S.; Hopkins, D.A.; Geula, C. Neurobiology of butyrylcholinesterase. *Nat. Rev. Neurosci*. **2003**, 4, 131-138. doi: 10.1038/nrn1035.
9. Perry, G.; Cash, A.D.; Smith, M.A. Alzheimer Disease and Oxidative Stress. *J. Biomed. Biotechnol*. **2002**, 2,120-123. doi: 10.1155/S1110724302203010.
10. Tolnay, M.; Probst, A. REVIEW: tau protein pathology in Alzheimer's disease and related disorders. *Neuropathol. Appl. Neurobiol*. **1999**, 25, 171-187. doi: 10.1046/j.1365-2990.1999.00182.x.
11. Tripathi, M. K.; Sharma, P.; Tripathi, A.; Tripathi, P.N.; Srivastava, P.; Seth, A.; Shrivastava, S. K. Computational exploration and experimental validation to identify a dual inhibitor of cholinesterase and amyloid-beta for the treatment of Alzheimer's disease. *J. Comput. Aided. Mol. Des*. **2020**, 34, 983–1002. doi: 10.1007/s10822-020-00318-w.
12. Sharma, P.; Srivastava, P.; Seth, A.; Tripathi, P. N.; Banerjee, A. G.; Shrivastava, S. K. Comprehensive review of mechanisms of pathogenesis involved in Alzheimer's disease and potential therapeutic strategies. *Prog. Neurobiol*. **2019**, 174, 53–89. doi: 10.1016/j.pneurobio.2018.12.006.
13. Zatta, P.; Drago, D.; Bolognin, S.; Sensi, S. L. Alzheimer's disease, metal ions and metal homeostatic therapy. *Trends Pharmacol. Sci*. **2009**, 30, 346–355. doi: 10.1016/j.tips.2009.05.002.
14. Birks, J. Cholinesterase inhibitors for Alzheimer's disease. *Cochrane Database Syst. Rev*. **2006**, 25, CD005593. doi: 10.1002/14651858.CD005593.
15. Geula, C.; Darvesh, S. Butyrylcholinesterase, cholinergic neurotransmission and the pathology of Alzheimer's disease. *Drugs Today (Barc)* **2004**, 40, 711-721. doi: 10.1358/dot.2004.40.8.850473.
16. Ibrahim, M. M.; Gabr, M. T. Multitarget therapeutic strategies for Alzheimer's disease. *Neural Regen. Res*. **2019**, 14, 437-440. doi: 10.4103/1673-5374.245463.
17. Belluti, F.; Rampa, A.; Piazzi, L.; Bisi, A.; Gobbi, S.; Bartolini, M.; Andrisano, V.; Cavalli, A.; Recanatini, M.; Valenti, P. Cholinesterase inhibitors: xanthostigmine derivatives blocking the acetylcholinesterase-induced beta-amyloid aggregation. *J. med. Chem*. **2005**, 48, 4444–4456. doi: 10.1021/jm049515h.
18. Rizzo, S.; Cavalli, A.; Ceccarini, L.; Bartolini, M.; Belluti, F.; Bisi, A.; Andrisano, V.; Recanatini, M.; Rampa, A. Structure-activity relationships and binding mode in the human acetylcholinesterase active site of pseudo-irreversible inhibitors related to xanthostigmine. *ChemMedChem* **2009**, 4, 670-679. doi: 10.1002/cmdc.200800396.
19. Kozurkova, M.; Hamulakova, S, Gazova Z, Paulikova H, Kristian P. Neuroactive Multifunctional Tacrine Congeners with Cholinesterase, Anti-Amyloid aggregation and neuroprotective properties. *Pharmaceuticals (Basel)* **2011**; 4:382–418. doi: 10.3390/ph4020382.
20. Youdim, M.B. Multi target neuroprotective and neurorestorative anti-Parkinson and anti-Alzheimer drugs ladostigil and m30 derived from rasagiline. *Exp Neurobiol*. **2013**, 22, 1-10. doi: 10.5607/en.2013.22.1.1.
21. Amit, T; Avramovich-Tirosh, Y.; Youdim, M.B.; Mandel, S. Targeting multiple Alzheimer's disease etiologies with multimodal neuroprotective and neurorestorative iron chelators. *FASEB J*. **2008**, 22, 1296-1305. doi: 10.1096/fj.07-8627rev.
22. Saadeh, H.A.; Sweidan, K.A.; Mubarak, M.S. Recent advances in the synthesis and biological activity of 8-hydroxyquinolines. *Molecules* **2020**, 25, 4321. doi: 10.3390/molecules25184321.
23. Saadeh, H.A.; Sweidan, K.A.; Mubarak, M.S. Recent advances in the synthesis and biological activity of 8-hydroxyquinolines. *Molecules* **2020**, 25, 4321. doi: 10.3390/molecules25184321.
24. Radwan, A.A.; Alanazi, F.K.; Raish, M. Design and synthesis of multi-functional smallmolecule based inhibitors of amyloid-β aggregation: Molecular modeling and in vitro evaluation. *PLoS ONE* **2023**, 18, e0286195. doi: 10.1371/journal.pone.0286195.
25. Battisti, A.; Piccionello, A.P.; Sgarbossa, A.; Vilasi, S.; Ricci, C.; Ghetti, F, et al. Curcumin-like compounds designed to modify amyloid beta peptide aggregation patterns. RSC Advances 2017; 7:31714–31724. https://doi.org/10.1039/C7RA05300B. doi. 10.1039/C7RA05300B
26. Earl, C.; Bagneris, C.; Zeman, K.; Cole, A.; Barrett, T.; Savva, R. *Nucleic Acids Res.* **2018**, 46, 4286-4300. doi: 10.1093/nar/gky217.
27. Chalupova, K.; Korabecny, J.; Bartolini, M.; Monti, B.; Lamba, D.; Caliandro, R. et al. Novel tacrine-tryptophan hybrids: Multi-target directed ligands as potential treatment for Alzheimer's disease. *Eur. J. Med. Chem*. **2019**, 168, 491-514. doi: 10.1016/j.ejmech.2019.02.021.
28. Zou, Y.; Li, L.; Chen, W.Y.; Chen, T.T.; Ma, L.; Wang, X.; Xiong, B.; Xu, Y.C.; Shen, J. Virtual screening and structure-based discovery of indole acylguanidines as potent beta-secretase (BACE1) inhibitors. Molecules 2013, **18**, 5706-5722. doi: 10.3390/molecules18055706.
29. Case, D.A.; Aktulga, H.M.; Belfon, K.; Ben-Shalom, I.Y.; Berryman, J.T., Brozell, S.R., et al., Amber **2023**, University of California, San Francisco.

 doi:10.20944/preprints202402.0731.v1